Distribution Agreement

In presenting this thesis as a partial fulfillment of the requirements for a degree from Emory University, I hereby grant to Emory University and its agents the non-exclusive license to archive, make accessible, and display my thesis in whole or in part in all forms of media, now or hereafter now, including display on the World Wide Web. I understand that I may select some access restrictions as part of the online submission of this thesis. I retain all ownership rights to the copyright of the thesis. I also retain the right to use in future works (such as articles or books) all or part of this thesis.

Seyed Arshiya Namazi March 23, 2022

Optimizing the performance efficiency of highly polyvalent DNA-based motors

by

Seyed Arshiya Namazi

Khalid Salaita
Adviser

Department of Chemistry

Khalid Salaita

Adviser

Vincent Conticello

Committee Member

Brian Dyer

Committee Member

2022

Optimizing the performance efficiency of highly polyvalent DNA-based motors

By

Seyed Arshiya Namazi

Khalid Salaita

Adviser

An abstract of
a thesis submitted to the Faculty of Emory College of Arts and Sciences
of Emory University in partial fulfillment
of the requirements of the degree of
Bachelor of Science with Honors

Department of Chemistry

2022

Abstract

Optimizing the performance efficiency of highly polyvalent DNA-based motors

By Seyed Arshiya Namazi

Biological motors are at the core of all mechanical processes in biological systems as they convert chemical energy to mechanical work by hydrolyzing ATP. Recapitulating the properties of biological motors has been a goal of synthetic biology as it may allow for significant advancements in medicine and biotechnology. Addressing this, Yehl et al. have developed DNA-based motors that roll on an RNA chip and are among the fastest and most processive synthetic motors to date. However, the effect of parameters such as DNA leg length and enzyme concentration on the performance of the motors is largely unexplored. Here we analyze the relationship between motors with 12, 15, and 18 base pair (bp) leg-substrate lengths and motion output. Our results indicate that net displacement decreases with increasing leg length while processivity increases. DNA-based motors displaying 12 bp leg length were shown to deviate from self-avoiding random walk mechanisms that are demonstrated by 15 bp and 18 bp motors. We also show that the amount of substrate or fuel consumption increases with increasing DNA leg length. Finally, increasing enzyme concentration for motors with 18 bp leg length resulted in an increased displacement without sacrificing processivity. The findings presented in this work offer a guide towards constructing synthetic motors that could compete with biological motors and aid in the development of next generation sensors, robotics, and drug delivery.

Optimizing the performance efficiency of highly polyvalent DNA-based motors

By

Seyed Arshiya Namazi

Khalid Salaita

Adviser

A thesis submitted to the Faculty of Emory College of Arts and Sciences
of Emory University in partial fulfillment
of the requirements of the degree of
Bachelor of Science with Honors

Department of Chemistry

2022

Acknowledgements

I would like to thank Dr. Khalid Salaita for giving me the opportunity to conduct research in his lab. I never imagined that I would be able to work on topics as interesting as synthetic molecular motors. By allowing me into his lab and through his mentorship, I have been able to grow immensely as a scientist and meet many exceptional people that will serve as an inspiration to me throughout my life.

I would like to thank Selma Piranej for her mentorship and guidance while I worked in Dr. Salaita's lab. She is one of the most industrious and determined people that I have ever met, and I am thankful that she has pushed me to achieve more than I thought I would be able to accomplish.

I would like to thank Dr. Brian Dyer and Dr. Vincent Conticello for serving on my committee and for helping me to attain a foundation in biophysical and biomolecular chemistry. Their courses have allowed me to obtain a greater understanding of my own research.

Lastly, I would like to thank members of the Salaita lab for their support throughout my academic career and my pursuit of an honors thesis. I appreciate being able to be part of such an amazing community.

Table of Contents

Introduction

In biological systems movement is powered by molecular motors such kinesin, dynein, and myosin, allowing for mechanical processes such as cell division, muscle contraction, and cargo transport.[1] These proteins generate motion via conformational change through converting the chemical energy from ATP into mechanical energy by hydrolysis **(Fig. 1a-c).** Being able to replicate the properties of biological motors occurring in nature by using a ground up approach has been a longstanding goal of scientists.

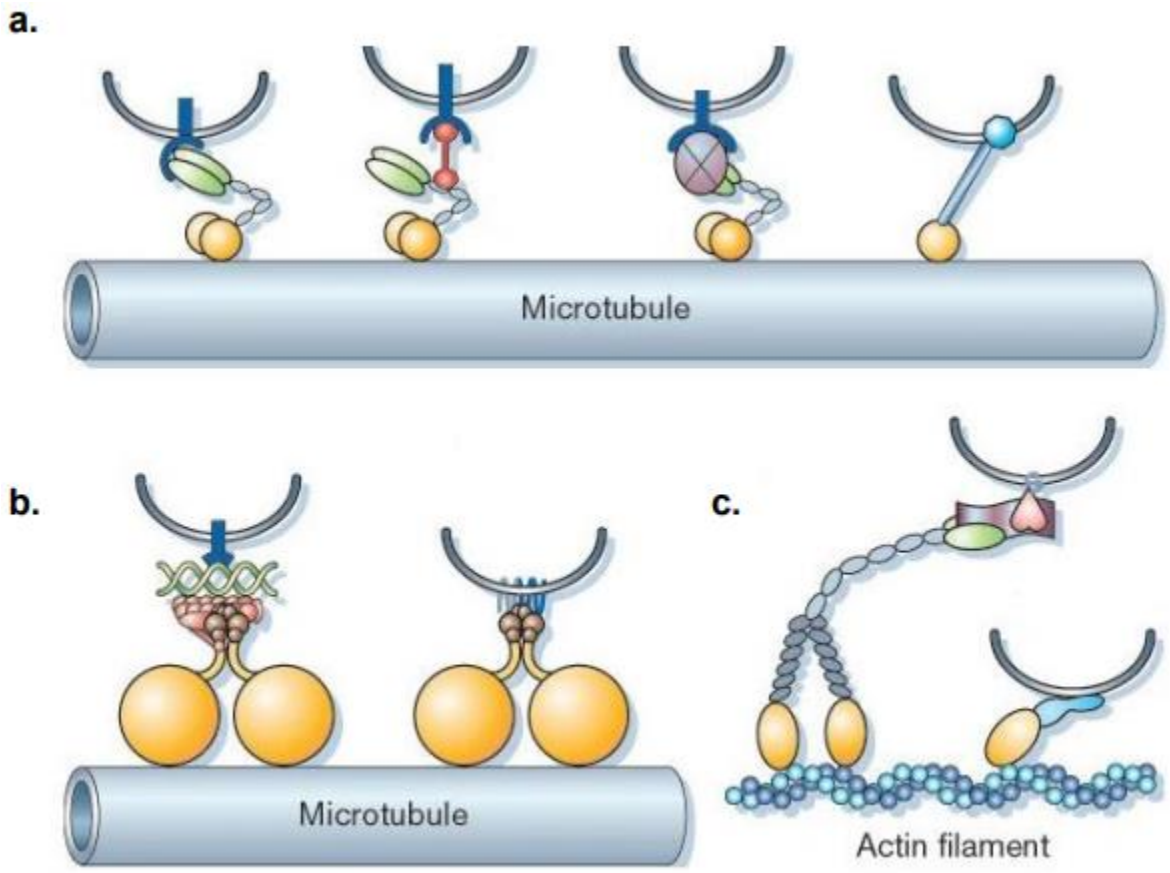

Figure 1. Molecular motors perform mechanical work via cargo transportation. a. kinesin. **b.** dynein. **c.** myosin.[1]

Early molecular machinery primarily consisted of two state systems such as cis-trans isomers, rotaxanes, pseudorotaxanes, and catenanes.[2-4] In the case of roxatanes, pseudoroxatanes, and catenanes, the system was biased towards one state, and upon receiving a chemical stimulus they were able to utilize chemical energy from that stimulus to shift towards the second state **(Fig. 2a-c)**.[3, 5] In the case of cis-trans isomer systems, the stimulus consisted of primarily UV radiation which allowed for transition between states **(Fig. 3)**.[4] The limitations of these systems include difficulty to coordinate and incorporate into larger systems capable of achieving some function, in addition to being limited to only two states.[3] However, they successfully displayed that it is possible to convert chemical energy to mechanical motion which is a key component to biological motors as well as future synthetic motors.

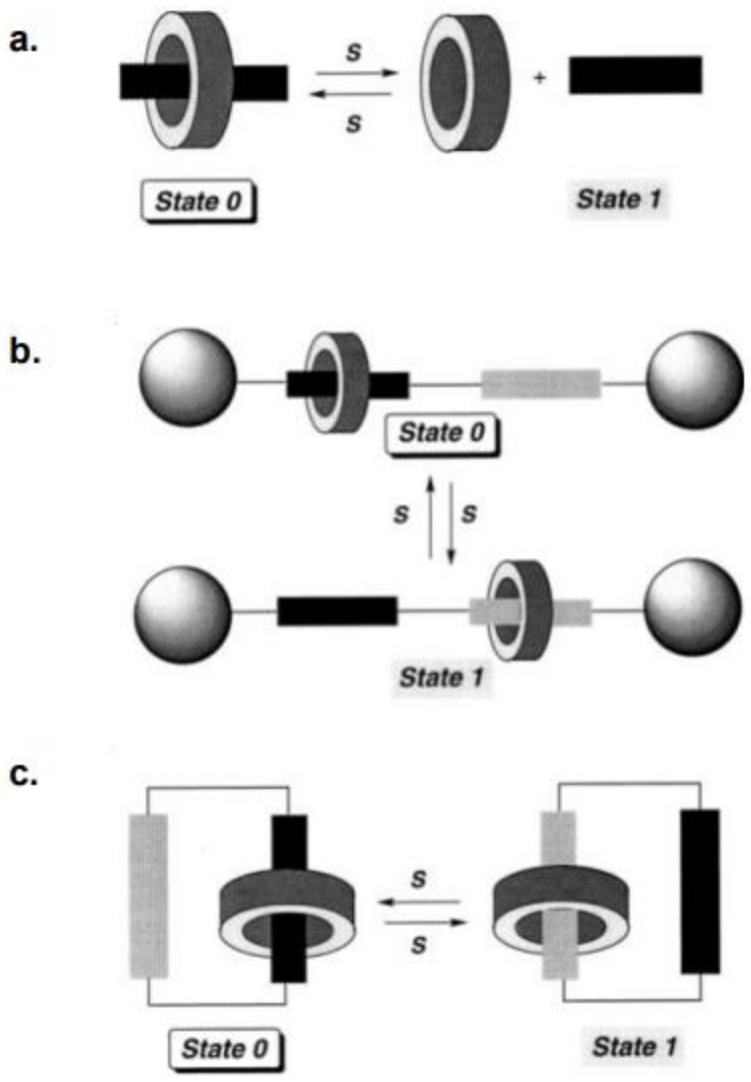

Figure 2. Two state molecular switch systems. a. pseudorotaxanes. **b.** rotaxanes. **c.** catenanes.[3]

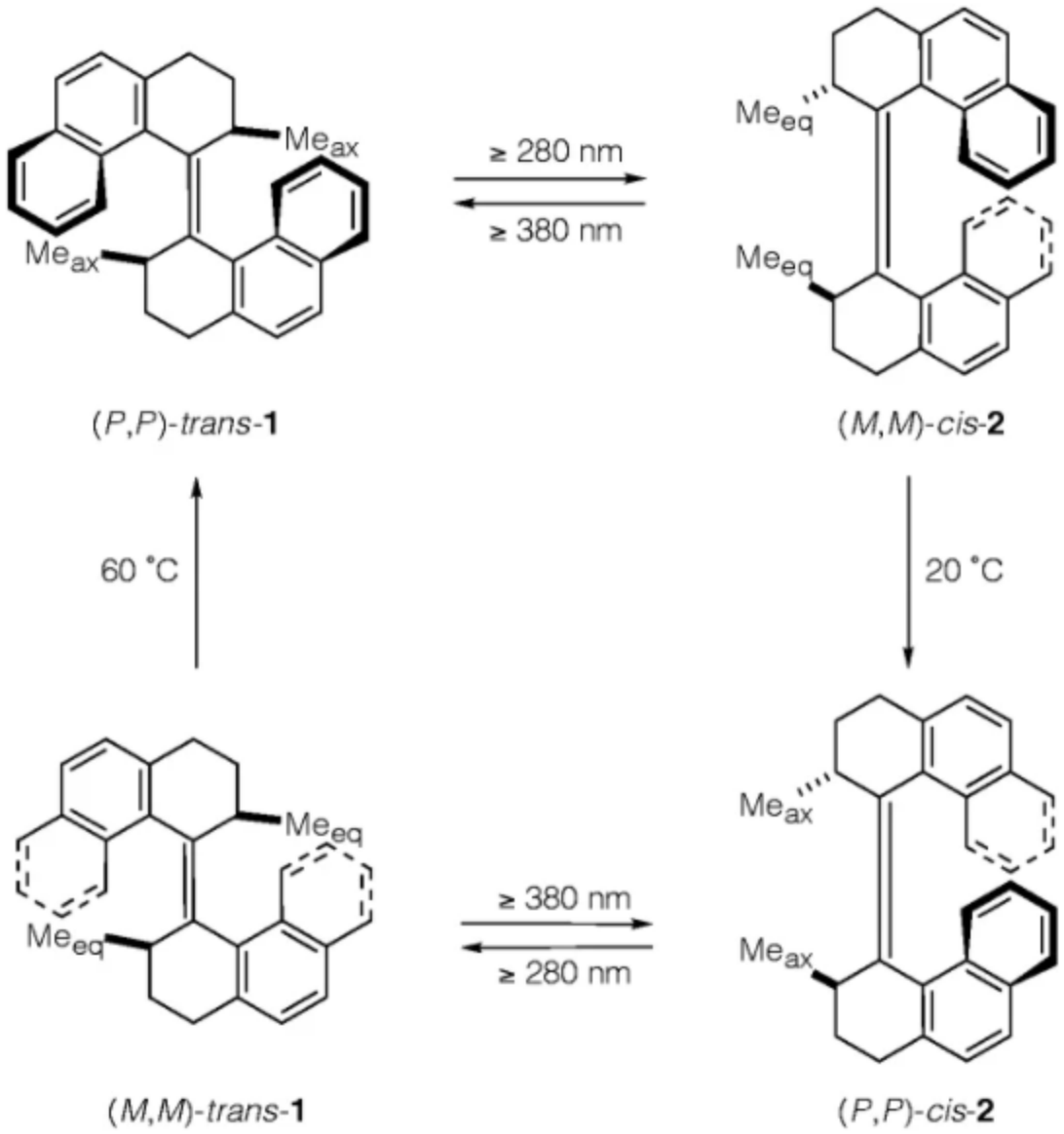

Figure 3. UV radiation triggered molecular rotor operating via cis-trans isomerization in order to produce motion.[4]

Scientists transitioned to DNA-based motors in order to develop complex systems capable of achieving more functions as compared previous molecular switch predecessors. The convenience of Watson-Crick base paring allows for ease of design in contrast to alternative methods such as amino-acid/peptide-based motors. Earlier

systems of DNA based motors primarily consists of DNA walkers **(Fig. 4a-c)**.[6-11] The method of obtaining chemical energy varies among each method though in principle, the idea behind transport was the same; DNA molecules traverse through substrate via the utilization of Gibbs free energy obtained from dissociation of fuel strands.

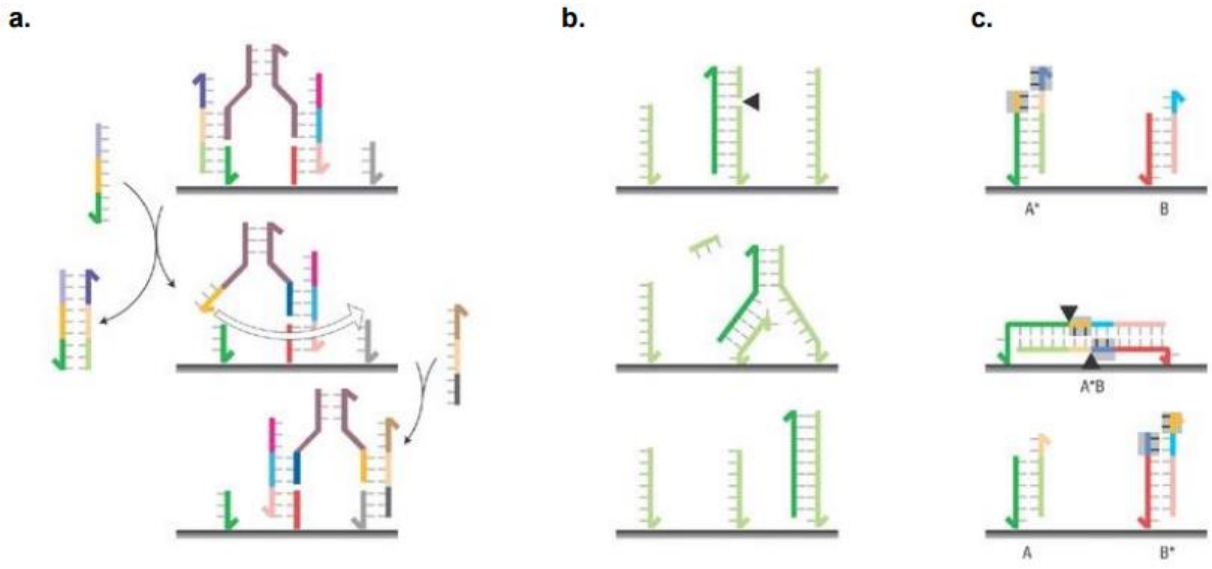

Figure 4. DNA walkers translocate through substrate tracks.[6] **a.** DNA walkers powered by strand displacement.[9] **b.** Walkers powered by hydrolysis of RNA/DNA backbone.[7, 10] **c.** Cargo transport of DNA powered by repeated cycle of hydrolysis and ligation.[11]

The transition from individual DNA walkers to more complex DNA spiders maintained the core principles behind motion generation while expanding on the mechanism by introducing multiple DNA legs.[12,13] This allowed for the benefit of decreasing the probability of motor dissociation. Additionally, molecular spiders had the benefit of autonomy and being able to interact with their environments by being able to carry out interactions upon some environmental trigger **(Fig. 5)**.[12]

Such systems were promising; however, the velocities of these motors were limited to approximately 1 nm min^{-1} due to the lack of coordination of DNA legs.[12] As a result, there was a trade-off between motor velocity and processivity. As the number of DNA legs increases, more binding events occur and the probability of motor dissociation decreases, however in this case due to the randomness of the binding, displacement is minimal.

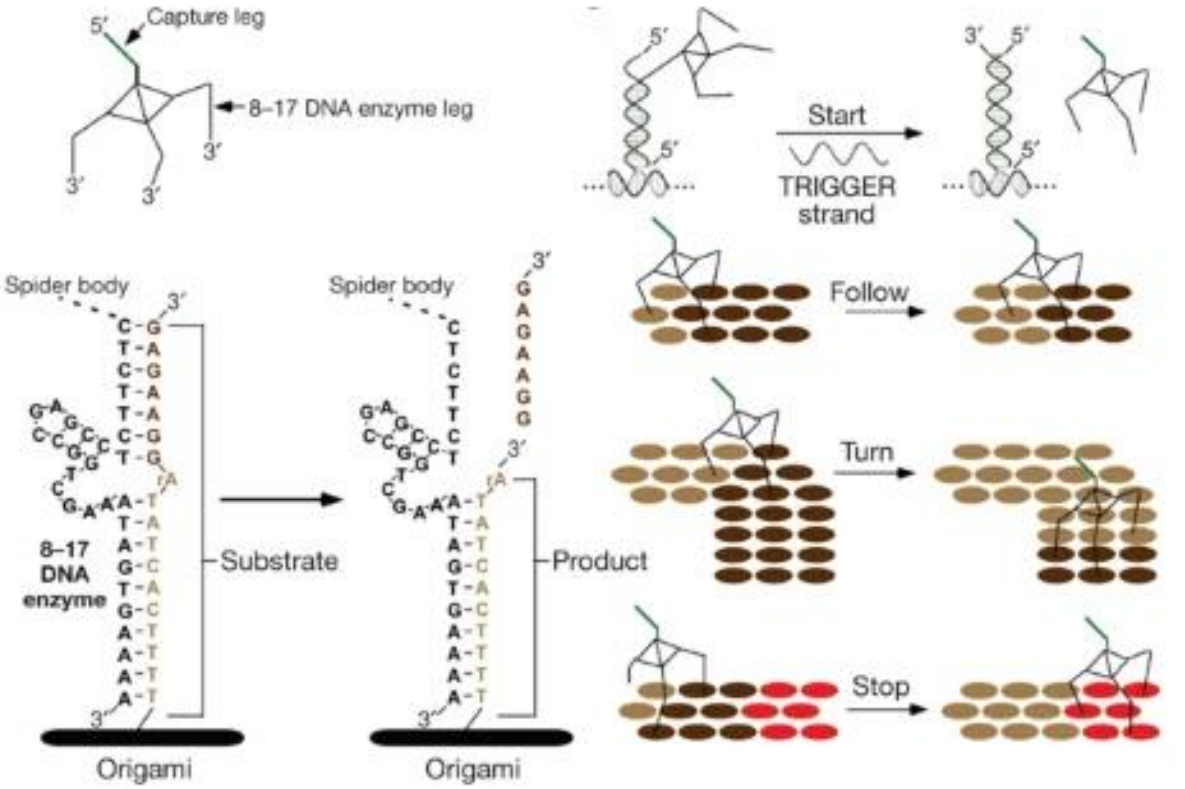

Figure 5. Multivalent DNA spiders are capable of executing follow, turn, and stop functions by responding to environmental stimulus.[12]

The development of rolling DNA-based motors powered by RNase H solved the problem of the lack of leg coordination through the utilization of a cog-and-wheel translocation mechanism which provided a boost in processivity and particle

displacement **(Fig. 6)**.[14] The high processivity is attributed to the high number of DNA legs that are present compared to predecessors. The high particle displacement is attributed to a combination of the high number of DNA legs as well as the fact that the association and dissociation from RNA fuel was able to be coordinated due to the mechanism of rolling which was allowed due to the spherical shape of the motor. The high particle displacement can also be attributed to the use of RNase H enzyme as the cleavage rate is multiple orders of magnitudes higher than DNAzyme and exonuclease counterparts that have been used in prior systems.[15, 16]

The DNA-based RNase H powered motors are composed of a silica core with DNA legs attached to via click chemistry. The DNA legs are composed of a poly-T spacer region, followed by a sequence that is complementary to the RNA fuel. On a gold surface, DNA molecules are adhered via gold-thiol chemistry. RNA/DNA chimera is then hybridized to the thiolated DNA oligonucleotide. The RNA component acts as the fuel for translocation being cleaved by RNAse H when hybridized to the DNA legs on the particle. The motors are capable of translocating approximately 2.5 μm over a 30 minute period with super diffusive alpha correlation coefficient values. Regarding the velocity of the motors, the three main factors to consider are k_{on} (DNA/RNA association), k_{off} (DNA/RNA dissociation), and k_{cat} (rate of enzyme cleavage). k_{on} and k_{off} are extremely difficult to measure, however, k_{cat} has been measured to be approximately 25 min^{-1}.

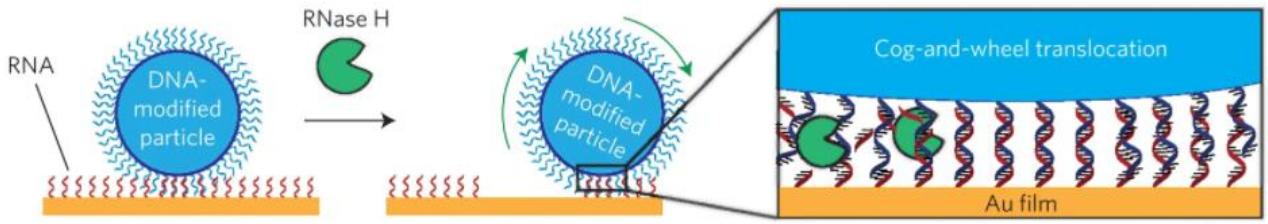

Figure 6. RNase H powered highly polyvalent DNA motors are capable of achieving translocation via cog-and-wheel mechanism. [14]

The current parameter space of this system can be further explored in order to alter the displacement, alpha correlation coefficients, and processivity of the motors. Previous experiments have revealed that decreasing the salt concentration allows for an increase in velocity due to decreased ionic strength destabilizing the RNA-DNA duplex formed by the motor legs binding to RNA substrate. The velocity is not dependent on k_{cat} past 0.4 min^{-1}, suggesting that k_{off} acts as the bottleneck rather than k_{cat} past a pH of 7.5. Enzyme concentration is capable of increasing particle velocity up to a point until processivity is largely decreased and the motors quickly dissociate from the tracks, with the optimal concentration of enzyme being 144 nM.

Further work by Bazrafshan et al. displays that outputs such as alpha correlation coefficients can also be altered by changing the shape of the motor from spherical to rod shaped **(Fig. 7a)**, which results in ballistic motion as revealed by trajectory analysis **(Fig. 7b)** and alpha correlation coefficient values close to 2 **(Fig. 7c)**.[17] Experiments performed with gold nanoparticle conjugates demonstrate an increase in velocity and processivity by increasing leg density, as well as an increase in processivity by increasing DNA leg

span **(Fig. 8)**.[18] These gold nanoparticle motors eventually became the fastest biological synthetic DNA motors to date.

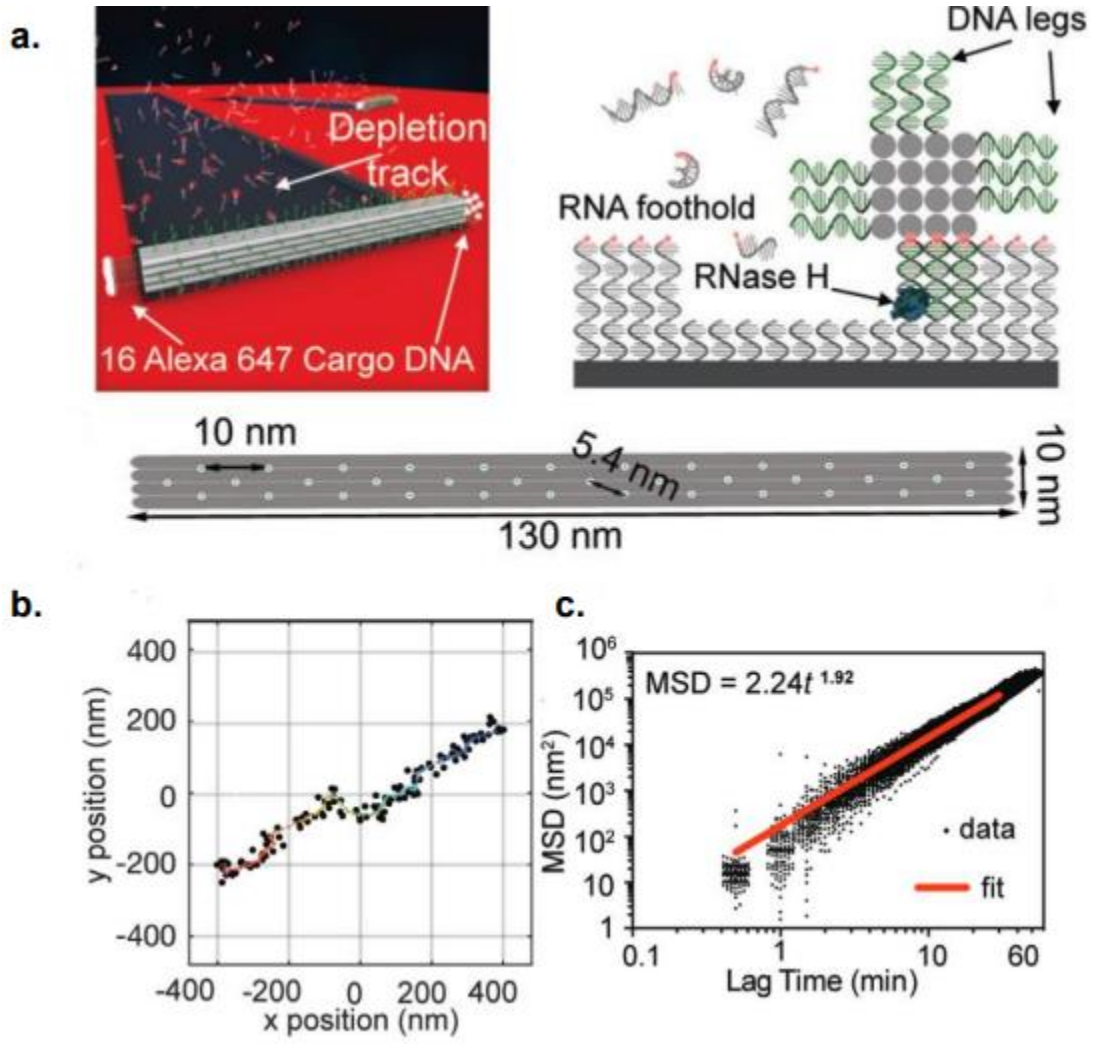

Figure 7. Rod-shaped DNA origami motors demonstrate ballistic motion.[17] **a.** Schematic representing mechanism of motion of rod-shaped DNA origami motors. **b.** Motors display linear trajectory. **c.** MSD vs lag time plot demonstrates alpha correlation coefficient close to 2.00.

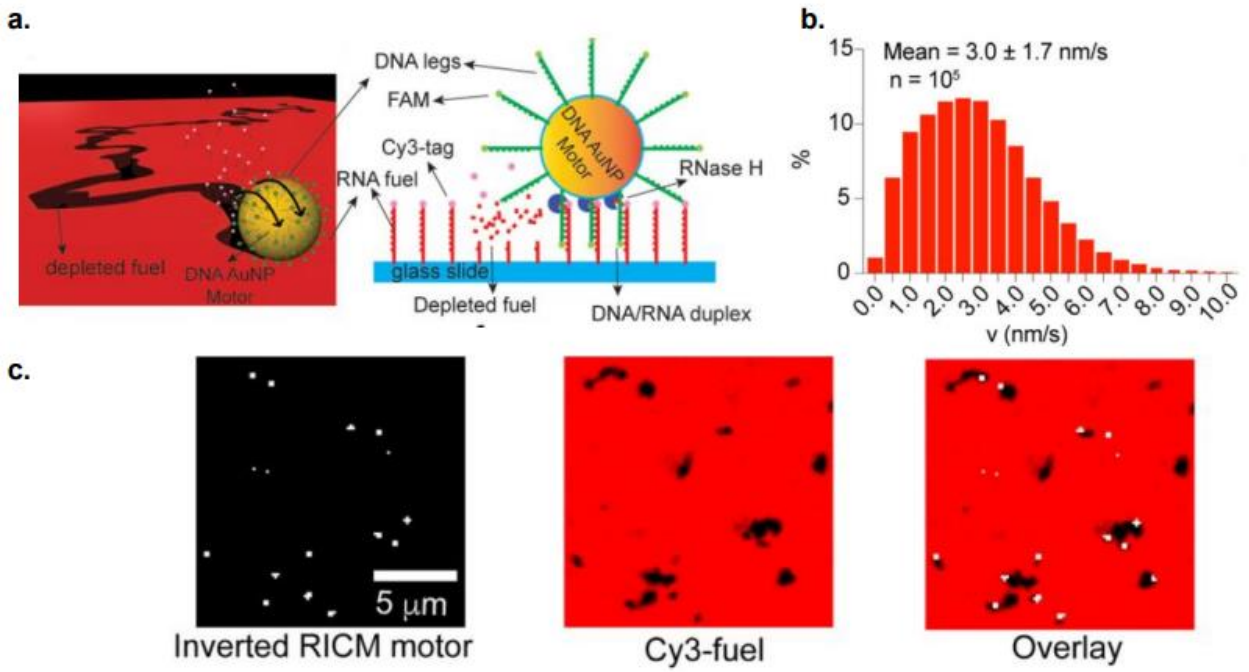

Figure 8. Particle translocation of gold nanoparticle derivative motors.[18] **a.** Schematic representing DNA gold nanoparticle motor transport. **b.** Distribution of motor velocities demonstrating fast nature of motors. **c.** Cy3 and RICM imaging demonstrating large tracks produced by DNA gold nanoparticle motors.

Though gold nanoparticle motors have been established to be the fastest and most processive, silica-based motors offer the advantage of practicality and applicability due to the fact that their large size allows them to be visualized with simple methods such as a cell phone microscope as shown by Yehl et al.[14] Thus, it would be justified to continue to explore the parameter space of silica-based motors with the hope of improving speed, processivity, and sensitivity in order to develop practical and label free sensing technologies. One parameter that has not been explored in particular is the impact of DNA sequence lengths on the performance of the DNA motors. In this work we explore the impact of increasing and decreasing the length of the DNA legs on the motor

displacement, velocity, and alpha correlation coefficients. To address this, we created different variations of the standard motors, each with varying DNA leg lengths and enzyme concentration. Minus the spacer region, the lengths of these DNA legs were 12, 15, and 18 base pairs long. Each of these motor types were subjected to the same conditions in order to evaluate their displacement, processivity, and alpha correlation coefficients. We hypothesized that the velocity would decrease with increasing leg length due to decreased k_{off} of the DNA duplex. Processivity however, was predicted to increase due to increased stability of RNA-DNA duplexes, resulting in lower probability of dissociation of the motors. Alpha values were hypothesized to stay the same with minor fluctuations as it was predicted that the burnt bridge Brownian ratchet mechanism would be preserved across all three motor types. We additionally explored the effects of varying enzyme concentrations to determine if the effects of increasing motor leg length can be undone.

Methods

The procedures involving thermal evaporation of gold films, fabrications of RNA monolayers, synthesis of azide-functionalized particles, synthesis of DNA motors, particle translocation powered by RNase H were directly adapted from the work of Yehl et al with minor variations.

Thermal evaporation of gold films:

A 25 x 75 mm No.1.5 glass slide was sonicated in DI water for 10 minutes, followed by a successive sonication in ethanol for 10 minutes. The slide was subsequently cleaned under a steam of N_2 gas. Using a thermal evaporator chamber, the slide was subjected to a pressure of 50 x 10^{-3} Torr. The chamber was then purged with N_2 three successive times and the pressure was reduced to 1-2 x 10^{-7} Torr by using liquid nitrogen and a turbo pump. After achieving the desired pressure, 1.5 nm of an adhesive chromium layer was deposited onto the slide at a rate of 0.2 Å s^{-1}, followed by 4 nm of Au at a rate of 0.2 Å s^{-1} which were both determined by a quartz-crystal microbalance. The Au coated samples were used within one week of evaporation.

Fabrication of RNA monolayers:

An IBIDI sticky-Slide VI0.4 flow chamber was adhered to the Au-coated slide to produce six channels (17 × 3.8 × 0.4 mm dimensions). The channels were washed with 10 mL of DI water. Next, a densely packed DNA monolayer was assembled onto the Au surface by using published protocols where 40 µl of a 1 µM 3′ -disulfide-modified DNA strand was incubated with the surface for 12 hours under a high ionic strength buffer of 1 M $KHPO_4$. Afterwards, excess DNA was removed via a wash with 10 mL of DI water. To

block any bare sites on the gold surface and maximize efficiency of RNA hybridization, each well on the surface was backfilled with 100 µl of a 100 µM SH(CH2)11(OCH2CH2)6OCH3 (SH-PEG) solution in ethanol and incubated for 6 hours. Excess SH-PEG was removed via a 10 mL wash with ethanol followed by a 10 mL wash with DI water. Lastly, RNA substrate was immobilized to the surface through hybridization of 100 µl of a complementary RNA/DNA chimera (100 nM) in 1 × PBS for 12 hours. The wells were sealed with Parafilm in each incubation step to prevent evaporation.

Synthesis of azide-functionalized particles:

In order to remove impurities, 1 mg of 5 µm aminated silica beads (Bangs Laboratory) was washed with 1 mL of DI water and centrifuged at 15,000 revolutions per minute (r.p.m). The supernatant was discarded, and the wash was repeated one additional time. The beads were then mixed with 1 mg of *N*-hydroxysuccinimidyl azide heterobifunctional linker followed by dilution in 100 µl of dimethylsulfoxide (DMSO) and 1 µl of a 10x diluted triethylamine stock solution in DMSO. The reaction proceeded in the dark for 24 hours and the beads were purified by adding 1 mL of DI water followed by a centrifuge at 15,000 r.p.m for 5 minutes. The supernatant was discarded, and the process was repeated for a total of 7 times, with the last time being a centrifugation with the particles resuspended in 100 µl of DI water. 50 µl of supernatant was removed to yield an azide-modified particle stock solution which was stored at 4 °C in the dark.

Synthesis of DNA motors:

To synthesize DNA motors, 5 µl of azide-functionalized particles were combined with 5 µl of alkyne-modified DNA stock solution (5 nM) and diluted in 25 µl of DMSO. Next,

5 µl of a 2 M triethyl ammonium acetate buffer (pH 7.0) was added, followed by 4 µl of 5 mM stock ascorbic acid solution which acted as a reducing agent. The click reaction was initiated upon addition of 2 µl from a 10 mM Cu-TBTA (tris((1-benzyl-1*H*-1,2,3-triazol-4-yl)methyl)amine) stock solution in 55 vol% DMSO. The newly synthesized motors were purified by seven total washes in which 1 mL of 10 % Triton-X and 1 x PBS were added, followed by a 5-minute centrifugation at 15,000 rpm after which the supernatant was removed. For the fourth to sixth wash, the motors were resuspended in 1 mL of 1 x PBS. For the final wash, the particles were resuspended in 100 µl of 1 X PBS. 50 µl of supernatant was removed and to motors were stored at 4 °C in the dark.

Particle translocation powered by RNase H:

RNA-substrate surfaces were washed with 1 mL of PBS in order to remove unbound RNA/DNA chimera. DNA functionalized particles were hybridized to the surface by diluting 5 µl of DNA-functionalized particle stock with 45 µl of 1 x PBS and adding it to the surface and letting incubate for 5 minutes. Unbound particles were removed via a wash with 1 mL of 1 x PBS. After hybridization, particle translocation was initiated upon buffer exchange with 100 µl of RNase H reaction buffer (25 mM Tris pH 8.0, 8 mM NaCl, 47.5 mM KCL, 1.5 mM $MgCl_2$, 0.75 % (g ml^{-1}) Triton X, 10 µM DTT, 144 nM RNase H, and 1 X PBS).

Optical Microscopy:

Brightfield and fluorescence images were acquired on a fully automated Nikon Inverted Research Microscope Eclipse Ti2-E with the Elements software package (Nikon), an automated scanning stage, a 1.49 NA CFI Apo TIRF 100× objective, a 0.50 NA CFI60

Plan Fluor 20× objective, a Prime 95B 25mm sCMOS (scientific complementary metal-oxide semiconductor) camera for image capture at 16-bit depth, a SOLA SE II 365 Light Engine for solid state white light excitation source, and a perfect focus system used to minimize drift during timelapse. Fluorescence images of Cy3 tracks were collected using a TRITC filter set (Chroma #96321) with an exposure time of 100 ms. All imaging was conducted at room temperature.

Particle trajectory analysis:

Trajectories of particles were first analyzed via ImageJ software by first performing background subtraction on 30-minute videos taken via brightfield microscopy. The video was subsequently corrected for drift using a Stackreg plug-in followed by analysis of particle coordinates across all frames using a Mosaic plug-in. The generated coordinate data was then analyzed using a custom written python script in which the data was filtered to remove particles that were unable to be tracked for the full 360 frames. From this filtered list, 200 random particles were selected in order to generate particle trajectory plots in addition to calculating net displacement and mean squared displacement which was used to calculate alpha correlation coefficients for individual particles.

Results and discussion

Motor net displacement decreases with increasing leg length

First, we monitored the performance of the DNA motors by varying the length of the DNA motor legs (**Fig. 9**) and analyzing particle trajectories from a 30-minute time-lapse. We varied the DNA leg length ranging from 12, 15, and 18 bp. The DNA sequences of the DNA legs are listed in **Table 1** below. Particle tracking from brightfield imaging of the motors indicate that particle net displacement decreases with increasing DNA leg length. In addition to net displacement calculations **(Fig. 11a)**, this is also confirmed by particle trajectory plots **(Fig. 10a-c)**, which display decreased motion as leg length increases. BF and Cy3 track analysis **(Fig. 12)** additionally display decreased track length as leg length increases.

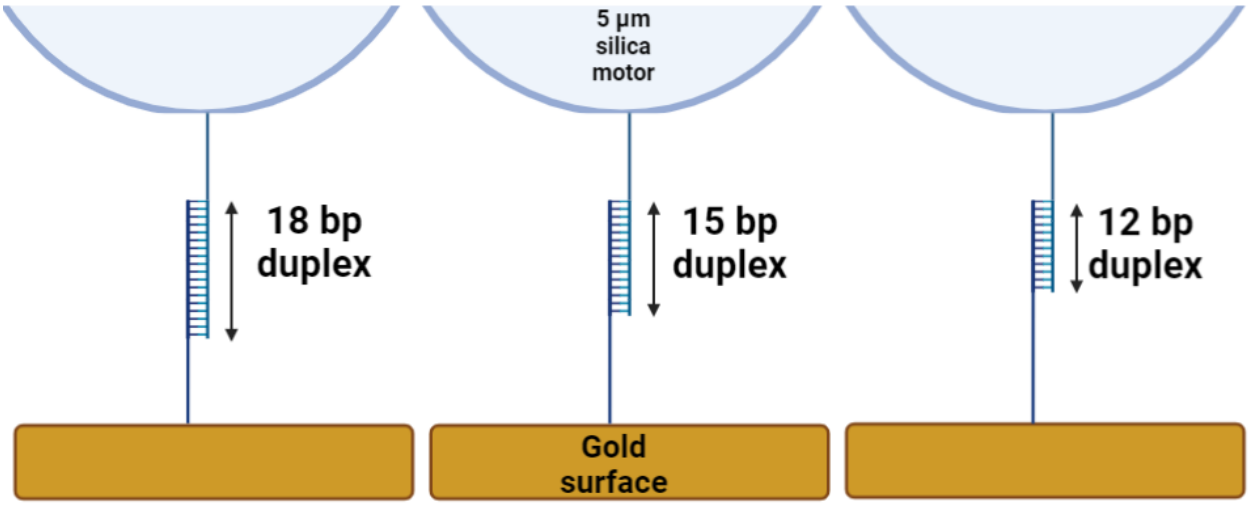

Figure 9. Scheme representing the three different motor types: 18 bp, 15 bp, and 12 bp duplex length (made with BioRender).

DNA anchor	/5AmMC6/GAGAGAGATGGGTGCTTTTTTTTTTTTTTT/3ThiolMC3-D/
RNA/DNA chimera substrate	GCACCCATCTCTCTCrCrCrCrCrCr**CrUrGrUrGrArUrUrGrArUrUrArCrU** /3Cy3Sp/
Particle DNA 9 bp	/5Hexynyl/TTTTTTTTTTTTTTTAGTAATCAA
Particle DNA 12 bp	/5Hexynyl/TTTTTTTTTTTTTTTAGTAATCAATCA
Particle DNA 15 bp	/5Hexynyl/TTTTTTTTTTTTTTTAGTAATCAATCACAG
Particle DNA 18 bp	/5Hexynyl/TTTTTTTTTTTTTTTAGTAATCAATCACAGGGG

Table 1. Sequences used in motor experiments.

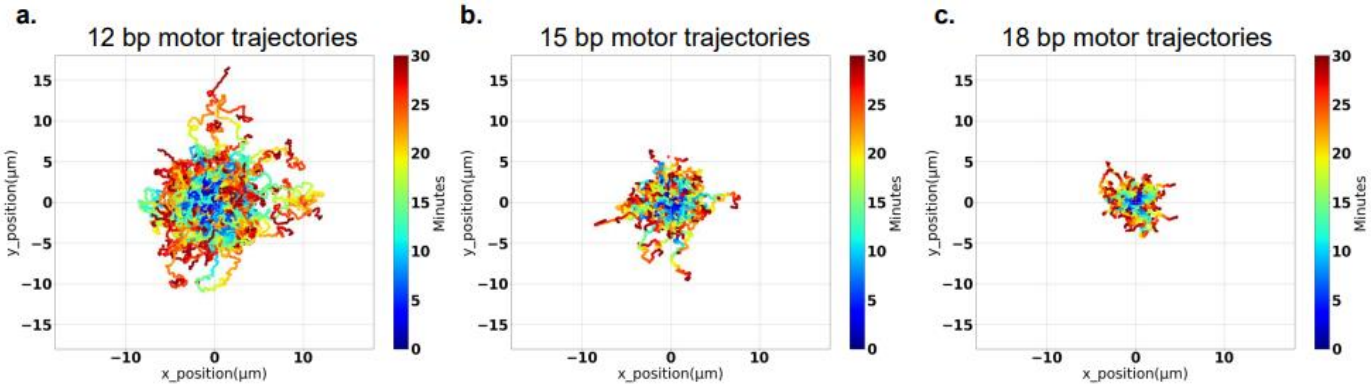

Figure 10. Motor trajectories display decreased motion as motor leg length increases (n=200). Ensemble particle trajectories plotted from the center (0,0) with color indicating time (0>30 mins), **a.** 12 bp motors **b.** 15 bp motors **c.** 18 bp motors.

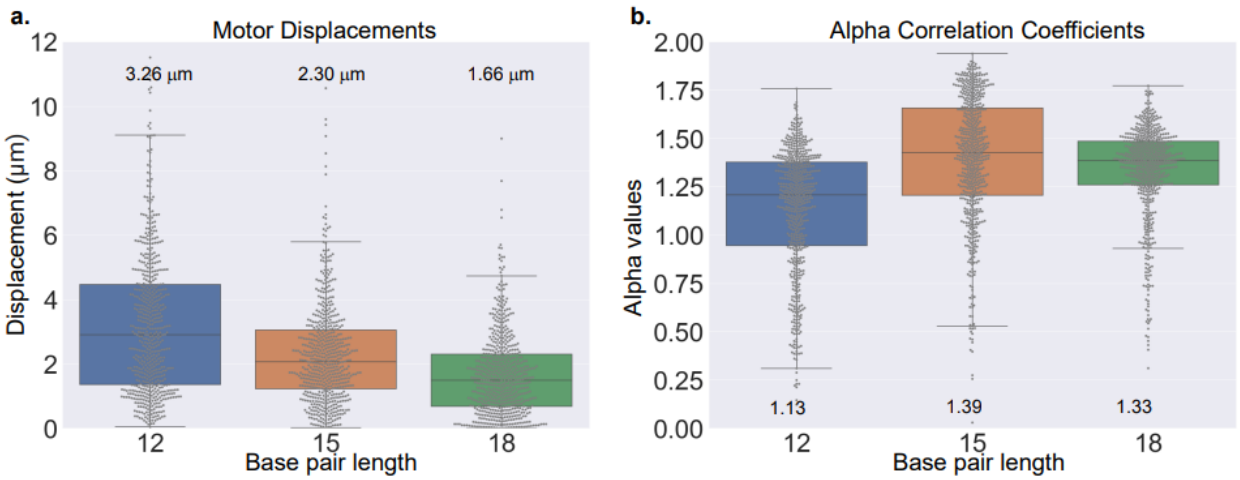

c.

Processivity		
12bp	15bp	18bp
60.8 %	80.3 %	83.2 %

Figure 11. DNA leg length impacts motor output (n=600). a. Motor net displacement after 30-minute time lapse decreases with increasing leg length. **b.** Motor alpha correlation coefficients remain constant for 15 bp and 18 bp motors while shifting towards diffusive values for 12 bp motors. **c.** Motor processivity defined as total percentage of particles remaining after 30-minute timelapse displays increase with increasing motor leg length.

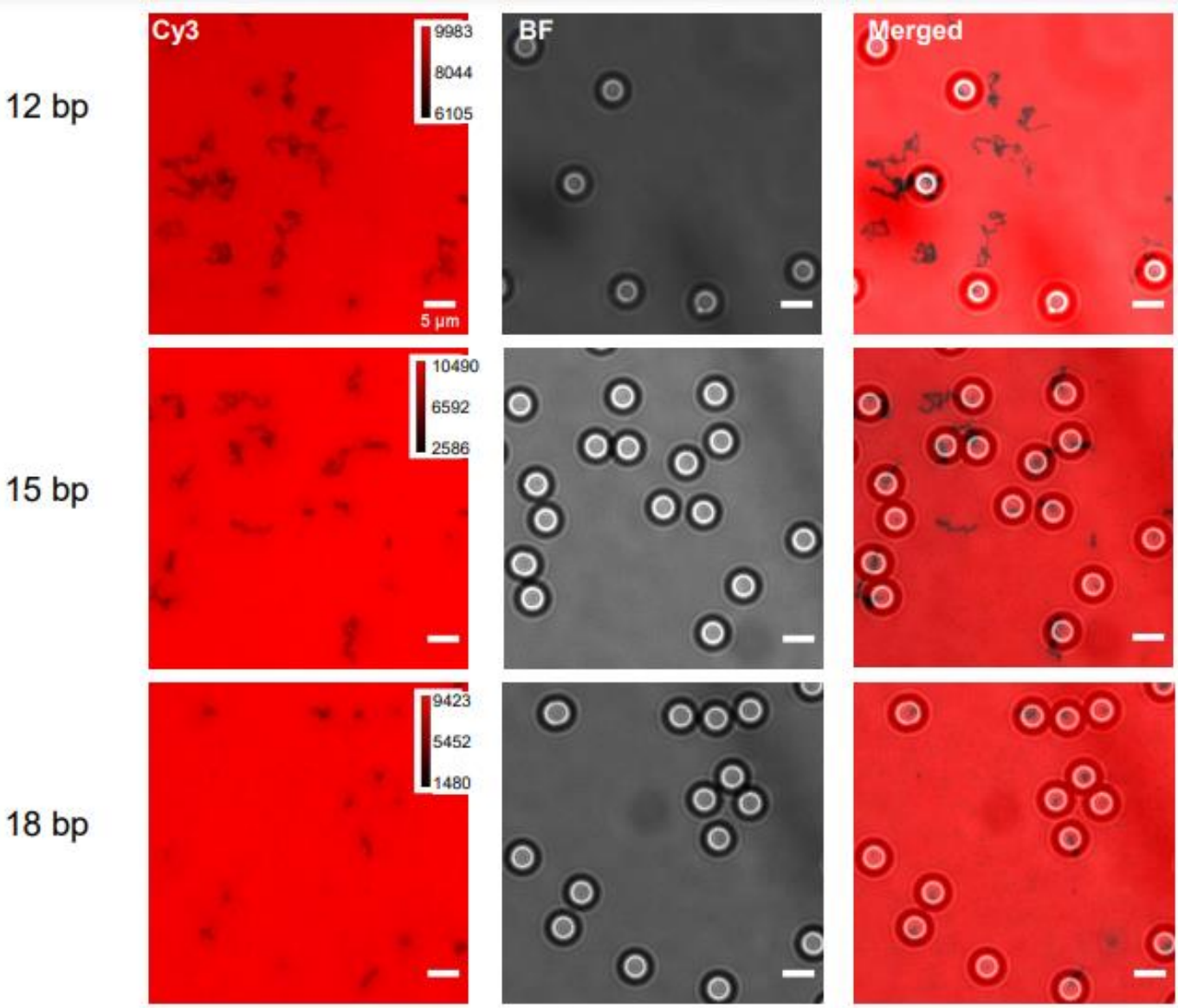

Figure 12. BF and Cy3 imaging after 30-minute timelapse for 12 bp, 15 bp, and 18 bp motors. Cy3 images displays tracks formed by the motors as substrate consumption has occurred. BF images displays location of motors. Merged imaging shows motors overlayed on Cy3 tracks to demonstrate substrate consumption of motors. Track lengths increase as motor length increases.

Processivity increases with increasing leg length

To determine processivity, we analyzed Cy3 and BF images taken after a 30 minute timelapse and determined the total number of motors still bound to a track as compared to the total number of tracks present. We concluded that processivity increases with increasing leg length **(Fig.11c and Fig.12)**. This suggests that the affinity of motor binding to substrate is largely determined by how strongly individual legs hybridize to RNA substrate. Since increased duplex length results in increased melting temperature, then the longer the leg length of the motors, the more stable the duplex, and the more processive the motor.

12 bp motors deviate from self-avoiding random walk

Upon initial glance, Cy3-RNA depletion tracks of 12bp motors looked noticeably thinner than those of 15bp and 18bp motors, potentially hinting at lower substrate consumption **(Fig. 12)**. To further analyze Cy3 tracks, we performed line scan analysis in which we compared Cy3 intensity of the tracks to their surrounding area to determine quantity of substrate consumed **(Fig. 13b)**.

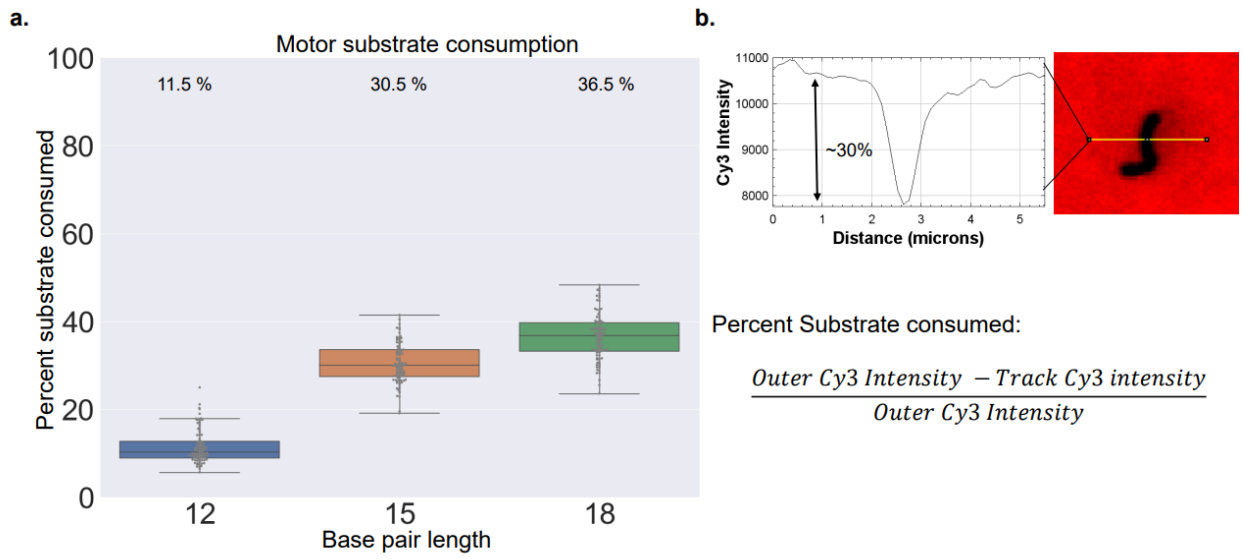

Figure 13. Substrate consumption by 12, 15, and 18 bp motors. a. Percent consumption of substrate at RNA depleted tracks display increased fuel consumption with increasing motor leg length **b.** Scheme displaying a visual demonstration of substrate consumption calculations where the Cy3 intensity of RNA-depleted tracks is compared to outer non-depleted regions.

Results indicate that on average, RNA fuel consumption is positively correlated with DNA leg length, with 12 bp consuming ~12% of substrate **(Fig. 13a)**. This suggests that strand dissociation events (k_{off}) before any cleavage events occur at a much higher rate when the formed RNA-DNA duplex is 12 bp long as compared to when it is 15 bp or 18 bp long. While 12 bp motors do generate tracks, it is likely that the motion is potentially a mixture of both rolling and hopping/sliding mechanism that are characteristics of instances where k_{off}/k_{cat}, or motor dissociation from tracks, is larger than k_{on}, referring to motor binding to tracks. This is further supported by the Brownian motion of the 12 bp motors indicated by alpha correlation coefficient data as the motors are shown to deviate from the self-avoiding random walk that is demonstrated by traditional 15 bp motors as

well as 18 bp motors **(Fig. 11b)**. Processivity data also supports this claim as increasing rate of dissociation events are one of the factors that can lead to decreased processivity in addition to decreasing rate of hybridization events **(Fig. 11c)**.

9 bp motors demonstrate minimal binding to surface

We also explored if decreasing leg length even further would result in further increased velocity and decreased processivity. To do this, we designed a DNA leg that would form a duplex of 9 bp in length when combined with RNA substrate. We visualized motion of these 9 bp motors under the same conditions as previous experiments.

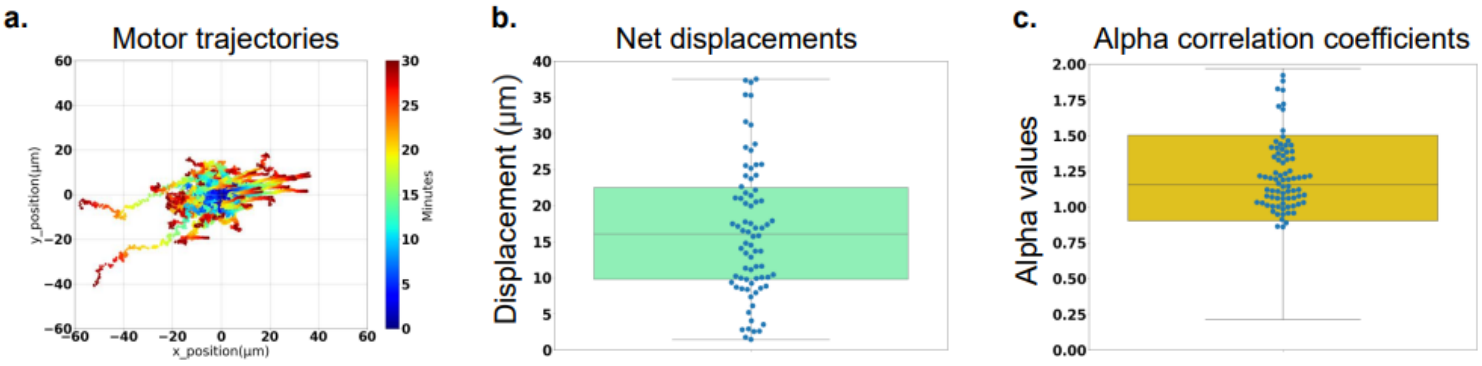

Figure 14. Analysis of 9 bp motors demonstrates minimal binding to surface (n= 73) a. Trajectory analysis of 9bp motors display motors unbound and floating in solution **b.** Net displacement calculations confirm lack of motor binding to substrate **c.** Alpha correlation coefficient values display Brownian motion.

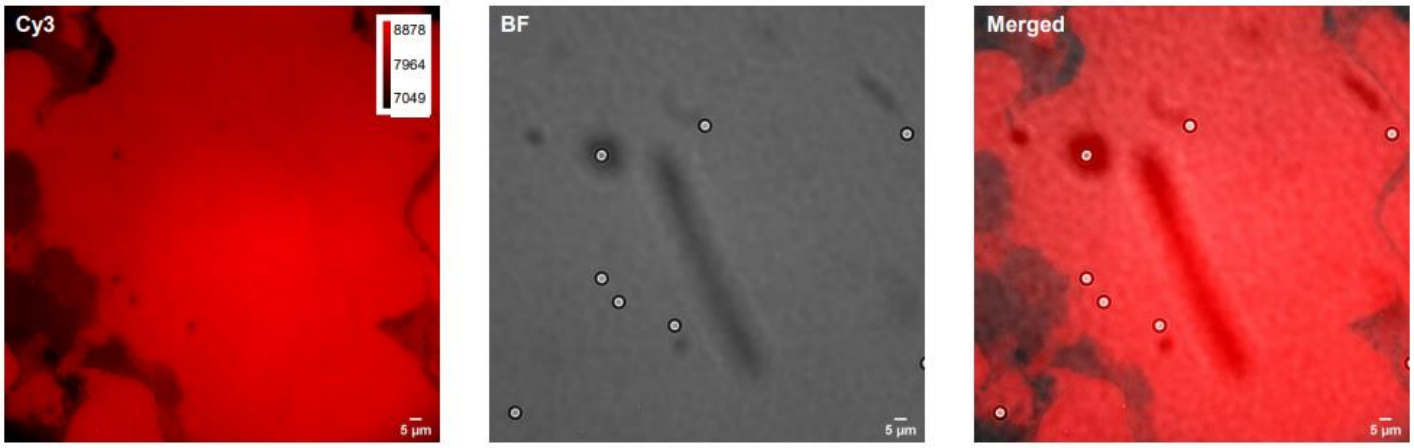

Figure 15. Visualization of BF and Cy3 tracks after 30-minute timelapse for 9 bp motors. Cy3 tracks display minimal substrate consumption. BF and overlayed imaging display small number of particles bound to surface.

Cy3 and BF track analysis indicate minimal fuel consumption and binding of DNA motors to tracks **(Fig. 15)**. This could be largely attributed to the second washing step that subsequently occurred after mobilization of motors to the surface, removing the vast majority of motors bound. Ultimately, some motors were able to bind to the surface and consume some fuel but had minimal motion **(Fig. 15)**. The number of particles detected in this analysis were very few, such that it is possible that the few motors in the track analysis were either defective as no motion was detected, or just about to dissociate from the surface and float towards a new site. The tracks created by these motors were very faint compared to those generated by any of the other motors. Brightfield analysis of motor trajectories indicated pure Brownian motion with a very large amount of displacement, indicating that particles were merely floating in solution, potentially very loosely bound to the surface, rather than rolling or hopping **(Fig. 14a-c)**. This indicates that the cutoff for an effective DNA motor leg length is somewhere between 12 bp and 9 bp, likely closer to

12 bp since we observe diminished activity of rolling mechanism already with 12 bp motors.

18 bp motors display increased velocity due to increased enzyme concentration

Since increasing leg length to 18 bp led to a decrease in velocity, then increasing enzyme concentration may have the potential to undo the effects of increased leg length by increasing the frequency of cleavage events, which should result in a higher k_{off} and increased velocity. We performed experiments with the 18 bp motors where we added 6 units (173 nM), 7 units (202 nM), and 10 units (288 nM) of enzyme instead of the standard 5 units (144 nM).

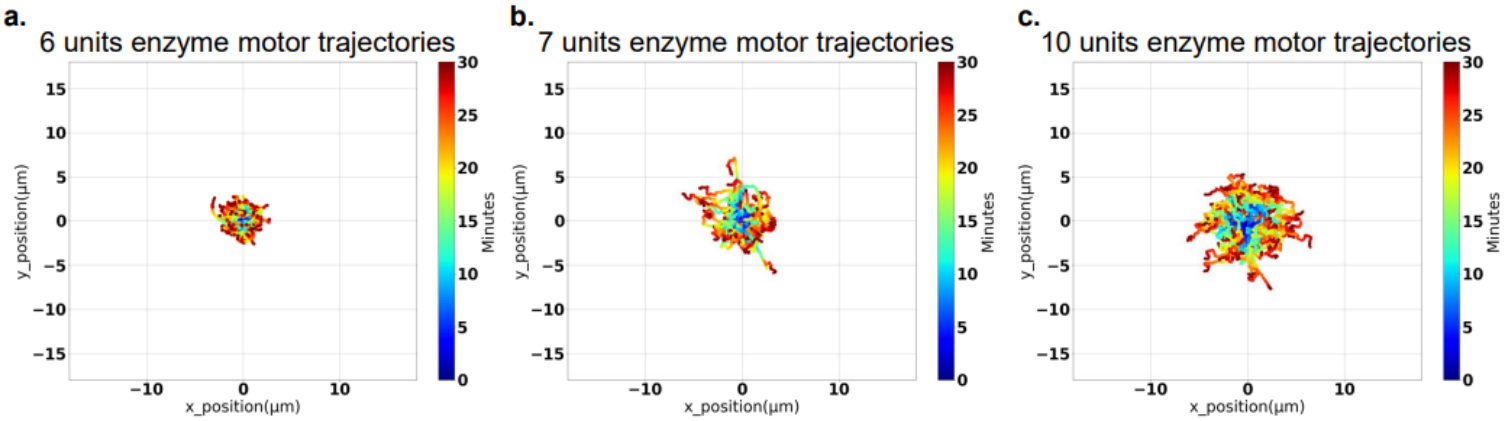

Figure 16. 18 bp motor trajectories display increased motion as RNase H concentration increases (n=200). Ensemble particle trajectories plotted from the center (0,0) with color indicating time (0>30 mins) for **a.** 6 units enzyme (173 nM) **b.** 7 units enzyme (202 nM) **c.** 10 units enzyme (288 nM)

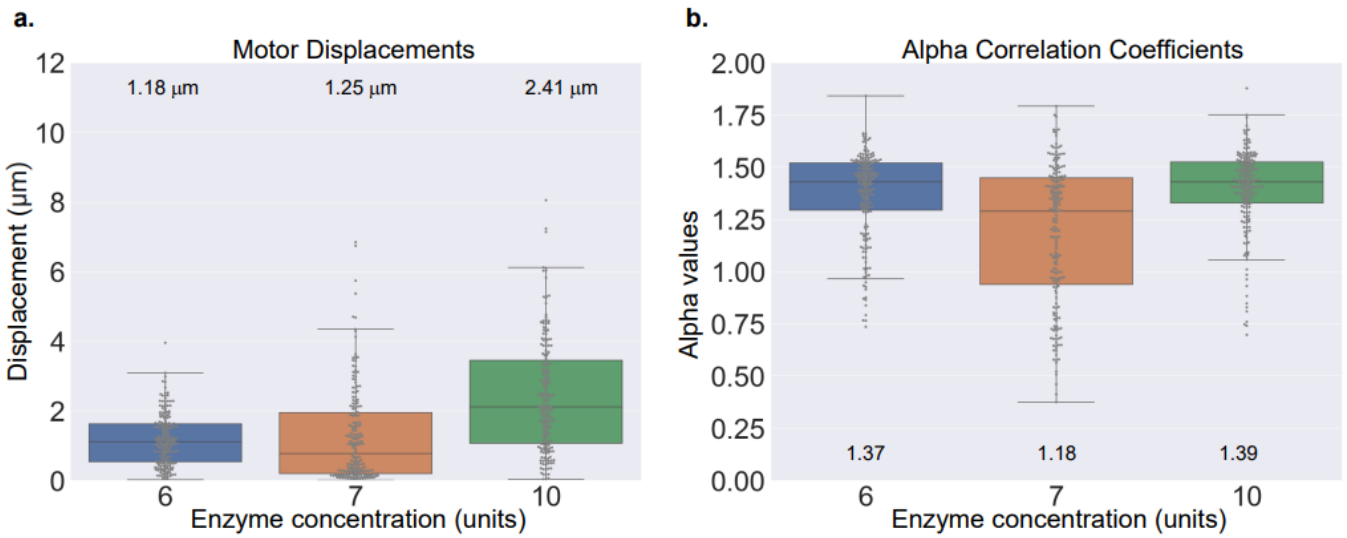

c.

Processivity		
6 units	7 units	10 units
78.0 %	79.8 %	81.5 %

Figure 17. Enzyme concentration impacts 18 bp motor output (n=200). a. Motors demonstrate increased net displacement as enzyme concentration increases after 30-minute time lapse. **b.** Particle alpha correlation coefficients remain constant throughout various enzyme concentrations. **c.** Motor processivity, defined as total number of particles remaining after 30-minute timelapse, remains constant throughout different enzyme concentrations.

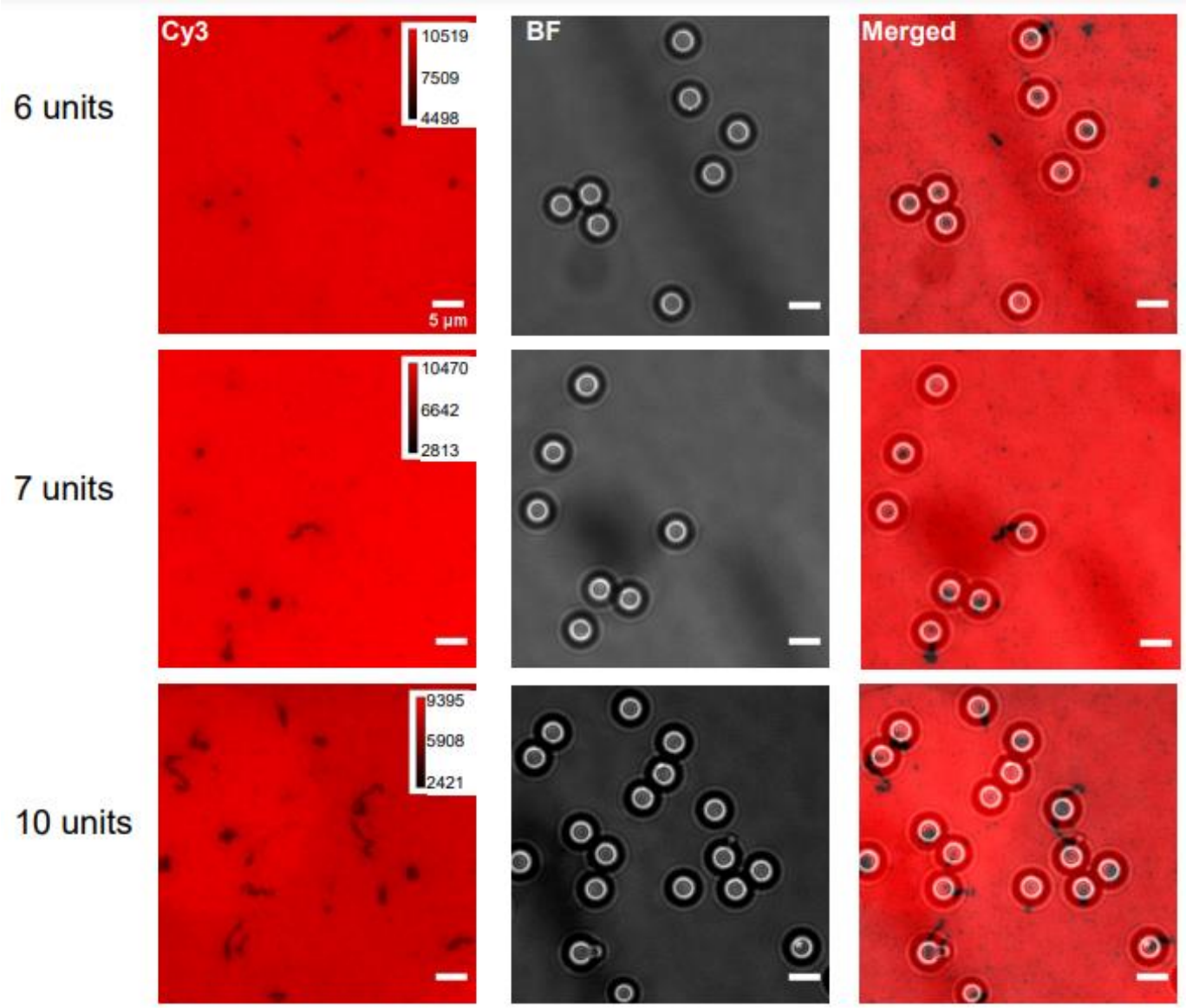

Figure 18. Visualization of BF and Cy3 tracks after 30-minute timelapse for 18 bp motors at RNase H concentrations 173 nM (6 units), 202 nM (7 units), and 288 nM (10 units). Cy3 imaging displays consumed substrate regions. BF imaging displays bound DNA motors. Overlayed imaging demonstrates substrate consumption by DNA motors. Tracks display slight increase in length from 6 to 7 units of enzyme and large increase compared to other groups at 10 units of enzyme.

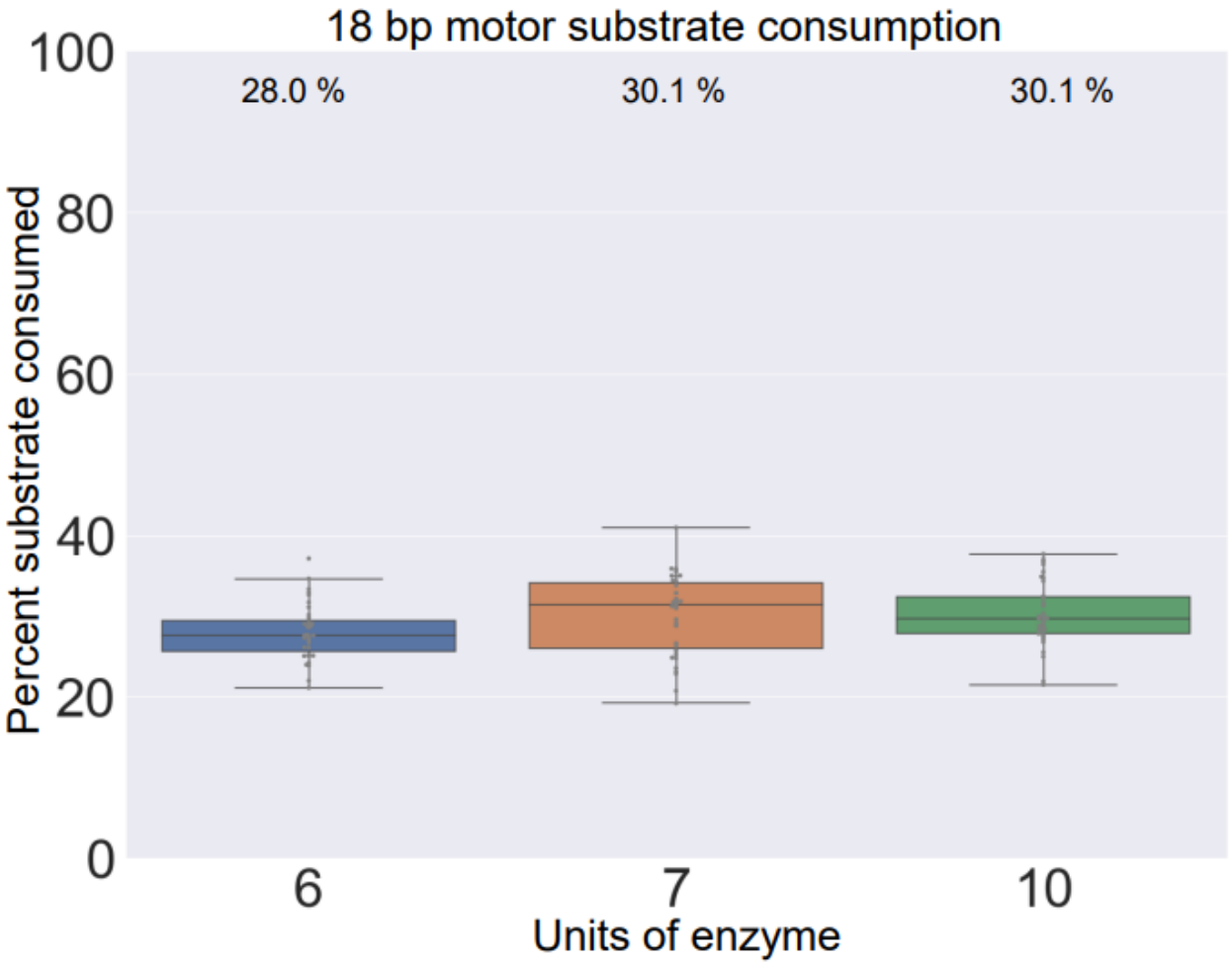

Figure 19. 18 bp motors demonstrate constant amount of substrate consumption. 18 bp motor Cy3 tracks were analyzed in the same manner as DNA leg length experiments. Results indicate minimal fluctuations in percentage of RNA consumed with varying enzyme concentrations.

18 bp motors display an increase in displacement with increasing enzyme concentration with the difference between motor performance at 6 and 7 units of enzyme concentration being minimal **(Fig. 17a)**. This difference was confirmed by both particle trajectories and Cy3 tracks **(Fig. 16a-b, 17)** Displacement increased significantly at 10 units of enzyme, producing an average that is approximately the same as those of 15 bp

motors **(Fig. 11a)** as indicated by both motor trajectories and substrate track lengths **(Fig. 16c, 17a, 18).** Surprisingly, processivity was not impacted by increasing enzyme concentrations **(Fig, 17c, 18)** suggesting that duplex stability at initial binding is an important factor determining processivity. This is additionally confirmed by substrate consumption data which displays minimal fluctuation as enzyme concentration is increased (**Fig.19**). Similarly, alpha correlation coefficient values did not vary throughout enzyme concentrations with an exception being at 7 units of enzyme likely due to error as seen by larger distribution compared to other enzyme units **(Fig. 17b).**

Motor output is likely influenced by k_{off}

As previously mentioned, motor speed depends on three factors, DNA leg binding to RNA substrate, cleavage of RNA substrate, and dissociation of DNA motor leg (k_{on}, k_{cat} , k_{off} respectively). A change in velocity suggests that at least one of these variables is being altered as a result of changing leg lengths. Literature on DNA binding kinetics reveals that alteration of sequence lengths does not have significant impact on k_{on} but decreasing length results in exponential increase of k_{off}.[19-21] Alternatively, k_{on} has a dependence on sequence composition.[19, 22, 23] Based on this information, we can rule out any change being made to k_{on} values. This leaves us with k_{off} and k_{cat} being the potential changing factors impacting velocity and displacement.

DNA-RNA duplexes exist as A form DNA which generally tends to restrict sequence information from being accessed by enzymes. However, even sequence non-specific enzymes such as RNase H have some degree of sequence specificity. Previous literature displays that the enzyme prefers cleavage in the middle of a CAAG sequence downstream of a G rich sequence.[24] Compared to average sequences, this leads to an

increased k_{cat}/K_m ratio of approximately 1.5 times in magnitude. In the context of our experiments however, it is unlikely that whatever bias the enzyme has towards the 15 bp motor sequence would be altered by addition or removal of triple base sequences **(Table 1)** because neither result in a significant/attractive sequence resembling the aforementioned CAAG sequence in the G rich context being created or eliminated. Therefore, it would be reasonable to assume that even if the enzyme is biased to cleave a specific site on the formed duplex, removal, or addition of triple bases would likely not influence that bias.

Motor dynamics are products of individual leg-substrate interactions

Recent efforts towards modeling microscale and nanoscale motors emphasize the elasticity of the components of the system in addition to the importance of k_{on} and k_{off} values on motor dynamics.[25, 26] However, such studies underemphasize the impact of higher k_{off} values. We propose that the dynamics of individual leg-substrate interactions can be used to understand emerging properties of DNA motors **(Fig. 20)**. In the case of velocity and fuel consumption, shorter DNA legs correspond to a net decreased rate of leg-substrate hybridization as a result of higher DNA-RNA duplex k_{off} values. This results in a decreased net total of cleavage events required for leg substrate dissociation, thus resulting in a smaller amount of time the motor remains bound to the substrate before rolling. This leads to the motors moving faster due to loose binding to the substrate. The decreased rate of hybridization and thus decreased amount of fuel consumption can also be used to explain deviation from burnt bridge Brownian ratchet mechanism as in the case of the 12 bp motors. Similarly, processivity can also be explained by higher k_{off} rates of individual duplexes leading to decreasing probability of leg-substrate hybridization.

Additionally, enzyme concentration data suggests that individual k_{off} values of leg-strand duplexes are the determining factor for initial binding of motors to surface, which explains substrate consumption data as well as processivity. However, successive cleavage of the duplex results in increasing k_{off} of individual duplexes as they get shorter, resulting in higher net displacement and velocity.

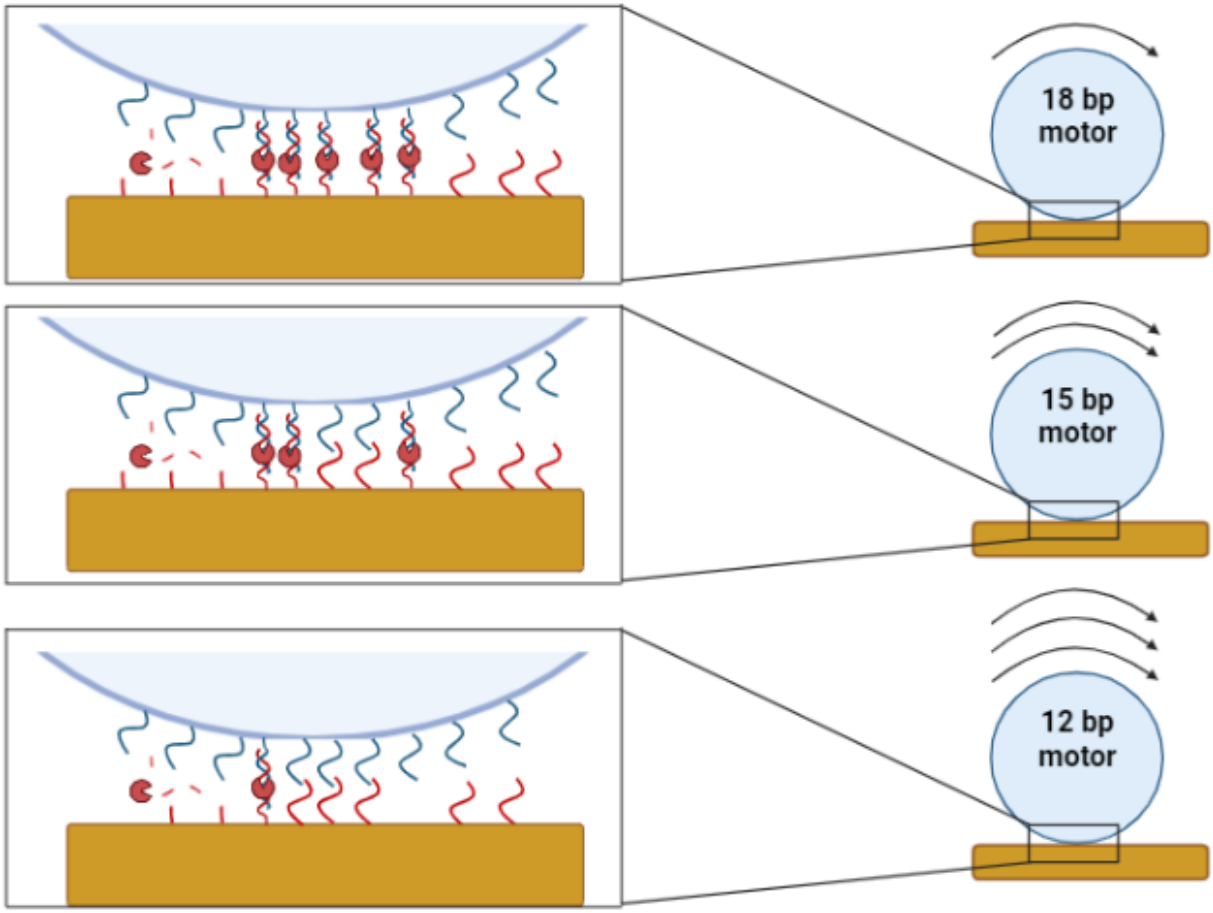

Figure 20. Scheme representing that decreased leg-substrate hybridization due to higher k_{off} values results in less required cleavage events for strand dissociation and thus faster velocity and net displacement (made with BioRender).

Conclusion and future directions:

This work uncovers previously unexplored parameter spaces of highly polyvalent DNA-based motors. We have shown that decreasing motor leg length allows for a larger net displacement through sacrificing the tightness of the binding of the motors with substrate leading towards decreased processivity and in deviation from a self-avoiding random walk mechanism as seen with 12 bp motors. This can be attributed to the collective increase of leg-substrate dissociation rates (k_{off}) that is caused by decreasing duplex length. We envision that this work can be incorporated into design of better particle sensing technology as our knowledge of the system parameter space increases.

In the future we wish to measure the force generation capabilities of 12 bp and 18 bp motors. 15 bp motors have been previously shown to demonstrate 100+ pN of force to perform tasks such as bond ruptures and nanopatterning.[27] Understanding the implications of leg length on force generation may allow for further optimization of motor capabilities. Additionally, we wish to explore the effect of altering DNA leg sequence on motor performance, as it may be a way of altering k_{on} which can subsequently be used for motor optimization.

References:

1. Schliwa, M.; Woehlke, G., Molecular motors. *Nature* **2003,** *422* (6933), 759-65.
2. Davis, A. P., Synthetic molecular motors. *Nature* **1999,** *401* (6749), 120-1.
3. Balzani, V.; Gomez-Lopez, M.; Stoddart, J. F., Molecular machines. *Acc. Chem. Res.* **1998,** *31* (7), 405-414.
4. Koumura, N.; Zijlstra, R. W. J.; van Delden, R. A.; Harada, N.; Feringa, B. L., Light-driven monodirectional molecular rotor. *Nature* **1999,** *401* (6749), 152-155.
5. Sauvage, J. P., Transition metal-containing rotaxanes and catenanes in motion: Toward molecular machines and motors. *Acc. Chem. Res.* **1998,** *31* (10), 611-619.
6. Bath, J.; Turberfield, A. J., DNA nanomachines. *Nat. Nanotechnol.* **2007,** *2* (5), 275-284.
7. Bath, J.; Green, S. J.; Turberfield, A. J., A free-running DNA motor powered by a nicking enzyme. *Angew. Chem. Int. Ed.* **2005,** *44* (28), 4358-61.
8. Wickham, S. F.; Endo, M.; Katsuda, Y.; Hidaka, K.; Bath, J.; Sugiyama, H.; Turberfield, A. J., Direct observation of stepwise movement of a synthetic molecular transporter. *Nat. Nanotechnol.* **2011,** *6* (3), 166-9.
9. Shin, J. S.; Pierce, N. A., A synthetic DNA walker for molecular transport. *J. Am. Chem. Soc.* **2004,** *126* (35), 10834-10835.
10. Tian, Y.; He, Y.; Chen, Y.; Yin, P.; Mao, C. D., Molecular devices - A DNAzyme that walks processively and autonomously along a one-dimensional track. *Angew. Chem. Int. Ed.* **2005,** *44* (28), 4355-4358.
11. Yin, P.; Yan, H.; Daniell, X. G.; Turberfield, A. J.; Reif, J. H., A unidirectional DNA walker that moves autonomously along a track. *Angew. Chem. Int. Ed.* **2004,** *43* (37), 4906-4911.
12. Lund, K.; Manzo, A. J.; Dabby, N.; Michelotti, N.; Johnson-Buck, A.; Nangreave, J.; Taylor, S.; Pei, R.; Stojanovic, M. N.; Walter, N. G.; Winfree, E.; Yan, H., Molecular robots guided by prescriptive landscapes. *Nature* **2010,** *465* (7295), 206-10.
13. Pei, R.; Taylor, S. K.; Stefanovic, D.; Rudchenko, S.; Mitchell, T. E.; Stojanovic, M. N., Behavior of polycatalytic assemblies in a substrate-displaying matrix. *J. Am. Chem. Soc.* **2006,** *128* (39), 12693-12699.
14. Yehl, K.; Mugler, A.; Vivek, S.; Liu, Y.; Zhang, Y.; Fan, M.; Weeks, E. R.; Salaita, K., High-speed DNA-based rolling motors powered by RNase H. *Nat. Nanotechnol.* **2016,** *11* (2), 184-90.
15. Fang, S.; Lee, H. J.; Wark, A. W.; Kim, H. M.; Corn, R. M., Determination of ribonuclease H surface enzyme kinetics by surface plasmon resonance imaging and surface plasmon fluorescence spectroscopy. *Anal. Chem.* **2005,** *77* (20), 6528-6534.
16. Yehl, K.; Joshi, J. R.; Greene, B. L.; Dyer, R. B.; Nahta, R.; Salaita, K., Catalytic Deoxyribozyme-Modified Nanoparticles for RNAi-Independent Gene Regulation. *ACS Nano* **2012,** *6* (10), 9150-9157.
17. Bazrafshan, A.; Meyer, T. A.; Su, H.; Brockman, J. M.; Blanchard, A. T.; Piranej, S.; Duan, Y.; Ke, Y.; Salaita, K., Tunable DNA Origami Motors Translocate Ballistically Over μm Distances at nm/s Speeds. *Angew. Chem. Int. Ed.* **2020,** *59* (24), 9514-9521.

18. Bazrafshan, A.; Kyriazi, M. E.; Holt, B. A.; Deng, W.; Piranej, S.; Su, H.; Hu, Y.; El-Sagheer, A. H.; Brown, T.; Kwong, G. A.; Kanaras, A. G.; Salaita, K., DNA Gold Nanoparticle Motors Demonstrate Processive Motion with Bursts of Speed Up to 50 nm Per Second. *ACS Nano* **2021,** *15* (5), 8427-8438.
19. Andrews, R., DNA hybridisation kinetics using single-molecule fluorescence imaging. *Essays Biochem* **2021,** *65* (1), 27-36.
20. Jungmann, R.; Steinhauer, C.; Scheible, M.; Kuzyk, A.; Tinnefeld, P.; Simmel, F. C., Single-Molecule Kinetics and Super-Resolution Microscopy by Fluorescence Imaging of Transient Binding on DNA Origami. *Nano Lett.* **2010,** *10* (11), 4756-4761.
21. Dupuis, N. F.; Holmstrom, E. D.; Nesbitt, D. J., Single-Molecule Kinetics Reveal Cation-Promoted DNA Duplex Formation Through Ordering of Single-Stranded Helices. *Biophys. J.* **2013,** *105* (3), 756-766.
22. Ouldridge, T. E.; Sulc, P.; Romano, F.; Doye, J. P.; Louis, A. A., DNA hybridization kinetics: zippering, internal displacement and sequence dependence. *Nucleic Acids Res.* **2013,** *41* (19), 8886-95.
23. Strauss, S.; Jungmann, R., Up to 100-fold speed-up and multiplexing in optimized DNA-PAINT. *Nat. Methods* **2020,** *17* (8), 789-791.
24. Kielpinski, L. J.; Hagedorn, P. H.; Lindow, M.; Vinther, J., RNase H sequence preferences influence antisense oligonucleotide efficiency. *Nucleic Acids Res.* **2017,** *45* (22).
25. Kowalewski, A.; Forde, N. R.; Korosec, C. S., Multivalent Diffusive Transport. *J. Phys. Chem. B* **2021,** *125* (25), 6857-6863.
26. Korosec, C. S.; Jindal, L.; Schneider, M.; de la Barca, I. C.; Zuckermann, M. J.; Forde, N. R.; Emberly, E., Substrate stiffness tunes the dynamics of polyvalent rolling motors. *Soft Matter* **2021,** *17* (6), 1468-1479.
27. Blanchard, A. T.; Bazrafshan, A. S.; Yi, J.; Eisman, J. T.; Yehl, K. M.; Bian, T.; Mugler, A.; Salaita, K., Highly Polyvalent DNA Motors Generate 100+ pN of Force via Autochemophoresis. *Nano Lett.* **2019,** *19* (10), 6977-6986.